Radio Observations of the Supermassive Black Hole at the Galactic Center and its Orbiting Magnetar

Rebecca Rimai Diesing

Honors Thesis

Department of Physics and Astronomy
Northwestern University

Spring 2017

Honors Thesis Advisor: Farhad Zadeh

Radio Observations of the Supermassive Black Hole at the Galactic Center and its Orbiting Magnetar

Rebecca Rimai Diesing
Department of Physics and Astronomy
Northwestern University

Honors Thesis Advisor: Farhad Zadeh
Department of Physics and Astronomy
Northwestern University

At the center of our galaxy a bright radio source, Sgr A*, coincides with a black hole four million times the mass of our sun. Orbiting Sgr A* at a distance of ∼3 arc seconds (an estimated 0.1 pc) and rotating with a period of 3.76 s is a magnetar, or pulsar with an extremely strong magnetic field. This magnetar exhibited an X-ray outburst in April 2013, with enhanced, highly variable radio emission detected 10 months later. In order to better understand the behavior of Sgr A* and the magnetar, we study their intensity variability as a function of both time and frequency. More specifically, we present the results of short (8 minute) and long (7 hour) radio continuum observations, taken using the Jansky Very Large Array (VLA) over multiple epochs during the summer of 2016. We find that Sgr A*'s flux density (a proxy for intensity) is highly variable on an hourly timescale, with a frequency dependence that differs at low (34 GHz) and high (44 GHz) frequencies. We also find that the magnetar remains highly variable on both short (8 min) and long (monthly) timescales, in agreement with observations from 2014. However, since that time, its flux density has increased by a factor of ∼2. The cause of this increase is unknown. Finally, we find that the magnetar's flux as a function of frequency decreases as a power law with an index of -3.1.

I. INTRODUCTION

The inner parsec of our galaxy is a dense and turbulent region characterized by extreme physics and a number of unique radio sources (see Figure 1). Most notably, these sources include Sgr A*, which coincides with a black hole four million times the mass of our sun [4]. Given its proximity to Earth, Sgr A* provides an excellent opportunity to study black hole accretion. What is more, its low mass relative to that of typical active galactic nuclei (AGN) results in a shorter dynamical timescale ($t_{dyn}^{BH}\ \alpha\ M^{BH}$), meaning that significant variability can be observed in a matter of hours [10]. While the steady component of Sgr A*'s emission is thought to be powered by accretion, the mechanism driving this variability is not well understood.

On 24 April 2013, while monitoring Sgr A*, the *Swift* telescope detected an X-ray outburst from a second, previously unknown source, PSR J1745-2900 [5]. The source was later identified as a magnetar. Characterized by high spin down rates and extremely strong magnetic fields (10^{14} - 10^{15} G), magnetars represent a rare class of pulsars. Even more unusual, of the 28 known magnetars, the galactic center magnetar is one of only four to exhibit pulsed radio emission [3] [6]. Its unique properties and close proximity to Sgr A* (∼3 arcseconds, or a projected 0.1 pc) open a new window to study the region surrounding the black hole [1]. Ten months after the magnetar's initial X-ray outburst, enhanced radio continuum emission was detected [9] and found to vary erratically during the subsequent four months [8]. As with Sgr A*, the mechanism driving this variability is not well understood.

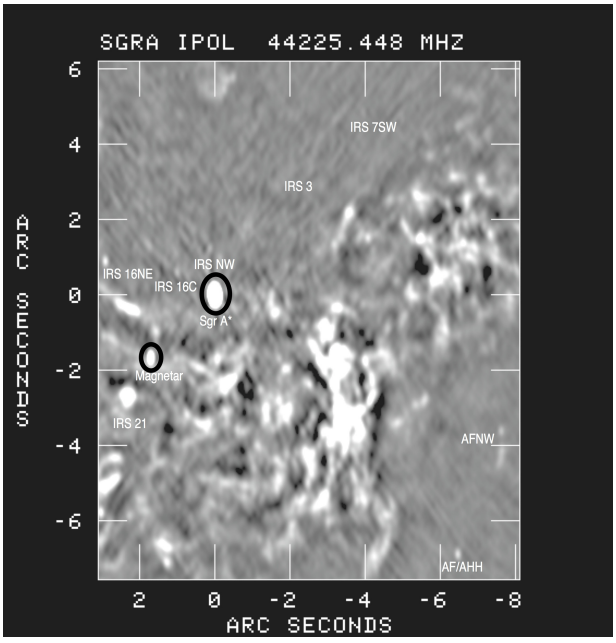

FIG. 1. Greyscale continuum image of Sgr A* and the magnetar (circled), taken with the VLA on 13 July 2016 (see Table II for observation parameters).

In order to better understand the behavior of Sgr A* and the magnetar, we study their intensity as a function of both time and frequency. While measurements of time variability inform models of flaring activity, measurements of frequency dependence reveal the energetics of a source. Specifically, the frequency variability of a

synchrotron source like Sgr A* corresponds to the energy spectrum of relativistic particles (electrons in our case). To make these measurements, we conducted radio observations over the summer of 2016 using the Jansky Very Large Array (VLA). These observations include both snapshot (8 min) and long (7 hour) observations, taken at multiple frequencies and over multiple epochs.

Although similar studies have been conducted in the past, these particular observations allow for a number of new measurements. First, though recent observations of the magnetar have been conducted, none have explored frequencies between between 8.35 and 87 GHz [7]. Since our observations were taken between 21 and 44 GHz, they probe a frequency regime that has not been recently monitored, and will improve our understanding of how the magnetar's behavior has changed since 2014. Second, previous measurements of Sgr A* and the magnetar's frequency dependences have been made by comparing observations taken over multiple epochs. The wide (8 GHz) bandwidth of our long observations allows us to instead measure flux density (a proxy for intensity) at multiple frequencies simultaneously. Given the time variability of Sgr A* and the magnetar, these simultaneous measurements will provide a more accurate picture of both sources' spectral and temporal behavior.

In Section II, we provide a more detailed discussion of our observations and data reduction techniques. In Section III, we present the results of these observations, including light curves (flux density vs. time) and spectra (flux density vs. frequency). Finally, in Section IV we discuss the implications of our results, as well as how future studies might expand upon this work.

II. OBSERVATIONS AND DATA REDUCTION

Using the VLA, we conducted two sets of observations: snapshot (8 min) and long (7 hour) . All observations were taken between June and August 2016. During this time, the VLA was in its second least compact (B) configuration, with a maximum distance of 11.1 km between antennas.

A. VLA Snapshot Observations

Four observations were taken between 2 June 2016 and 15 August 2016. Each observation lasted approximately one hour and covered 2 GHz of continuum bandwidth centered at 21.2, 32, and 41 GHz. For a given frequency setup, approximately 8 minutes were spent on-source. Amplitude gains were calibrated with respect to the flux calibrator 3C286, bandpass shapes were determined using J1733-1304 (also known as NRAO530), and phases were calibrated with respect to J1744-3116 (herein abbreviated to J1744). Observation parameters are listed in Table I.

To correct for phase instabilities due to Earth's atmosphere, we applied phase self-calibration. All flux density measurements of Sgr A* were taken from this phase-self calibrated data. However, due to high RMS noise, the magnetar was not visible in the phase self-calibrated images. For this reason, we also applied amplitude self-calibration to Sgr A*. We then obtained the flux density of the magnetar by fitting two-dimensional Gaussians to the amplitude self-calibrated images. It is also worth noting that, due to poor weather, the magnetar was not visible on 29 July 2016, even after amplitude self-calibration. On that day, we therefore present flux density measurements of Sgr A* alone.

Date	Band (GHz)	Bandwidth GHz	Synthesized Beam (PA) arcsec×arcsec (deg)
6 Jun 2016	K (21.2)	2	0.63 × 0.20 (168)
6 Jun 2016	Ka (32)	″	0.43 × 0.16 (11)
6 Jun 2016	Q (41)	″	0.33 × 0.12 (-172)
19 Jun 2016	K (21.2)	″	0.66 × 0.20 (14)
19 Jun 2016	Ka (32)	″	0.44 × 0.16 (12)
19 Jun 2016	Q (41)	″	0.34 × 0.13 (-171)
29 Jul 2016	K (21.2)	″	0.63 × 0.20 (168)
29 Jul 2016	Ka (32)	″	0.63 × 0.20 (168)
29 Jul 2016	Q (41)	″	0.63 × 0.20 (168)
15 Aug 2016	K (21.2)	″	0.67 × 0.26 (-14)
15 Aug 2016	Ka (32)	″	0.50 × 0.16 (-9)
15 Aug 2016	Q (41)	″	0.34 × 0.14 (-13)

TABLE I. VLA snapshot observation parameters.

B. VLA Long Observations

Two observations were taken on 13 July 2016 and 19 July 2016 as part of a multiwavelength observing campaign to monitor the variability of Sgr A*. Each observation lasted approximately seven hours and covered 8 GHz of continuum bandwidth centered at 44 GHz on 13 July and at 34 GHz on 19 July. As in the snapshot observations, amplitude gains were calibrated with respect to 3C286, bandpass shapes were determined using J1733-1304, and phases were calibrated with respect to J1744. Phase self-calibration was also applied. Observation parameters are listed in Table II.

Date	Band (GHz)	Bandwidth GHz	Synthesized Beam (PA) arcsec×arcsec (deg)
20160713	Q (44 GHz)	8	0.24 × 0.12 (3)
20160719	Ka (34 GHz)	″	0.35 × 0.15 (1)

TABLE II. VLA long observation parameters.

III. RESULTS

In the following section, we present light curves and spectra of both Sgr A* and the magnetar. Most notably, we find that Sgr A*'s spectral behavior differs from that found in previous studies, and that the magnetar has brightened by a factor of ∼2 since 2014. A more extensive summary of our findings can be found below.

A. Sgr A*

1. Light Curves

Figure 2 shows long-observation light curves of Sgr A* and phase calibrator J1744, with Sgr A*'s flux density averaged over 30 seconds. While the flux density of J1744 remains constant, Sgr A* exhibits significant variability on an hourly timescale, with a maximum of ∼20% change in flux on both dates.

Meanwhile, Figure 3 shows short-observation light curves of the same sources, with each light curve taken over the course of a single snapshot observation and frequency band. In order to maintain adequate signal to noise, Sgr A*'s flux density is averaged over 60 seconds. Since the calibrator J1744 was highly variable at 41 GHz, we will focus our analysis on the lower frequencies. From these light curves, we find that Sgr A* remains relatively stable over short (8 min) timescales, with any variability appearing as a smooth curve (see, for example, 29 July at 32 GHz).

Just as Sgr A*'s flux density varies with time, it is possible that its frequency dependence varies as well. Namely, Sgr A* might exhibit spectral behavior associated a non-variable quiescent component that differs from the spectral behavior associated with a variable flare component. To examine this possibility, Figure 4 shows sets of four light curves of Sgr A*, where each light curve represents 2 GHz of the total 8 GHz bandwidth. That being said, preliminary analysis does not show a clear relationship between time variability and frequency dependence.

2. Spectra

Figure 5 shows spectra of Sgr A* from both long observations. Spectra were taken by imaging 64 intermediate frequencies (IFs) individually, then fitting each image of Sgr A* to a 2D Gaussian. For each spectrum, the spectral index, α, was calculated using a least squares fit to the following function:

$$S = k\nu^{\alpha} \tag{1}$$

Thus, we assume that Sgr A*s spectrum follows a power law, as we would expect from a synchrotron source. Though α is positive at both bands, we find a significantly larger spectral index at 34 GHz ($\alpha = 0.68 \pm 0.007$ vs. $\alpha = 0.22 \pm 0.004$). This result is not consistent with spectral indices found across bands. Namely, Bower et. al. reports $\alpha = 0.28 \pm 0.03$ at frequencies between 1 and 40 GHz, but a larger spectral index, $\alpha = 0.5$ from 40 - 218 GHz [2]. Meanwhile, between bands, we estimate a spectral index of $\alpha = 0.62 \pm 0.005$, based on the following formula:

$$\alpha = \frac{\ln\left(S_Q^{ave}/S_{Ka}^{ave}\right)}{\ln\left(\nu_Q^{ave}/\nu_{Ka}^{ave}\right)} \tag{2}$$

Furthermore, the error was calculated as follows:

$$\sigma_\alpha = \sqrt{\frac{(\sigma_Q^{ave}/S_Q^{ave})^2 + (\sigma_{Ka}^{ave}/S_{Ka}^{ave})^2}{\ln\left(\nu_Q^{ave}/\nu_{Ka}^{ave}\right)}} \tag{3}$$

Once again, this spectral index is not consistent Bower et al. However, given the time variability of Sgr A*, this spectral index is likely less accurate than those taken within a single epoch.

B. Magnetar

1. Light Curves

Figure 6 shows light curves of the magnetar and Sgr A*, both averaged over entire epochs and as 8-minute, within-observation light curves, similar to those in Figure 3. On average, the magnetar has brightened by a factor of ∼2 since 2014. This increase aligns with the findings of Torne et al., which reports a factor of ∼6 decrease at low (2.54 - 8.35 GHz) frequencies, but a factor of ∼4 increase at high (87 - 291 GHz) frequencies [7]. Moreover, as the light curves show, the magnetar continues be highly variable, its fluctuations showing no obvious correlation with Sgr A*. Most notably, it varies significantly on short (8 min) timescales, while Sgr A* stays relatively flat. For example, consider the magnetar's behavior at K band on 15 August. While Sgr A* shows a maximum variation of ∼0.2% during the 8-minute interval, the magnetar varies by ∼59%.

2. Spectra

Figure 7 shows spectra of the magnetar and Sgr A*. To reduce noise in the magnetar spectrum, fluxes were averaged over groups of 8 IFs (i.e. each point covers 1 GHz bandwidth). Fitting to a power law gives negative spectral indices at both frequency bands. However, between bands, the spectral index is not statistically different from zero. Given the results of Torne et al., these spectral indices indicate a complex relationship between flux and frequency [7]. These results will be discussed further in the subsequent section of this paper.

IV. DISCUSSION AND CONCLUSION

Sgr A* continues to be a highly variable source, fluctuating significantly on an hourly timescale. While we cannot infer a model from VLA light curves alone, it is worth noting that infrared telescope Spitzer simultaneously observed Sgr A* on 13 and 19 July. Comparison of VLA and Spitzer light curves might aid in constraining a model for Sgr A*'s variability. For example, Yusef-Zadeh et. al. proposes that Sgr A*'s erratic behavior arises from synchrotron-emitting blobs of electrons, which cool adiabatically [10]. In this picture, emission would peak when the blob becomes optically thin. Since, in the case of adiabatic expansion, the time variability of optical depth depends on frequency, we would expect the amplitude and timescale of a flare to be similarly frequency-dependent [10].

Meanwhile, Sgr A*'s spectra present unanswered questions regarding the nature of Sgr A*'s energetics and optical depth. Given the disagreement between our result and that of Bower et al., further study is warranted. Such study might examine the time variability of Sgr A*'s spectral index, with the hope of determining whether Sgr A*'s spectrum can be explained in terms of quiescent and flaring components.

Turning to the magnetar, we find continued variability on both short and long timescales. In 2014, we explained this variability as synchrotron emission from a bow shock, produced as the outflow associated with the initial X-ray outburst collides with the surrounding interstellar medium (ISM). As the magnetar moves through the ISM, variations in ram pressure would produce variability in the observed flux density. Since it would take some time for the pressure of the cometary bubble supported by the outflow to equal the inward ram pressure, this model also explains the time delay between the initial X-ray outburst and enhanced radio emission. However, it does not explain the factor of $\sim$2 increase in the magnetar's flux density between 2014 and 2016. Thus, it remains unclear whether this increase is due to the variability of the magnetar's pulsed emission or the interaction between the outburst and the surrounding ISM.

Finally, our observations of the magnetar's spectrum indicate a complex frequency dependence that cannot be modeled by a simple power law. According to Torne et al., the magnetar exhibits a negative spectral index between 2.54 and 8.35 GHz, but a positive spectral index from 87 and 291 GHz. This discrepancy suggests that the spectrum changes direction at some point between 8.35 and 291 GHz. Hints of such a change, thought to be the result of incoherent emission becoming dominant, have been observed in other pulsars [7]. Since the fluxes found at 34 and 44 GHz are comparable to those found at high frequencies, we might infer that the magnetar's spectrum changed direction between 8.35 and 34 GHz. However, the negative spectral indices within both bands suggest that a more nuanced model is needed. It is also possible that the spectral behavior observed between frequency bands is simply the result of the magnetar's intrinsic time variability, since between-band spectra were taken over multiple epochs.

In summary, the galactic center is home to a number of unique and highly variable sources, the properties of which are not well understood. With further analysis, the light curves and spectra shown above can help constrain models of these sources' unusual behavior.

V. ACKNOWLEDGEMENTS

This work was supported by a grant from Northwestern University's Weinberg College of Arts and Sciences. The author wishes to thank the NRAO staff for instigating the observations used in this study. The National Radio Astronomy Observatory is a facility of the National Science Foundation operated under cooperative agreement by Associated Universities. The author also wishes to thank Lorant Sjowerman for his mentorship and assistance with data reduction.

[1] Bower, G. C., Deller, A., Demorest, P., et al. 2015, ApJ, 798, 120
[2] Bower, G. C., Markoff, S., Dexter, J., et al. 2015, ApJ, 802 69
[3] Camilo, F., Ransom, S. M., Halpern, J. P., et al. 2006, Nature, 442, 892
[4] Ghez, A. M., Salim, S., Weinberg, N. N., et al. 2008, ApJ, 689, 1044-1062
[5] Kennea, J. A., Burrows, D. N., Kouveliotou, C., et al. 2013, ApJ, 770, L24
[6] Levin, L., Bailes, M., Bates, S., et al. 2010, ApJ, 721, L33
[7] Torne, P., Desvignes, G., Eatough, R. P., et al. 2017, MNRAS, 465, 242-247
[8] Yusef-Zadeh, F., Diesing, R., Wardle, M., et al. 2015, ApJL, 811, L35
[9] Yusef-Zadeh, F., Roberts, D., Heinke, C., et al. 2014, The Astronomer?s Telegram, 6041, 1
[10] Yusef-Zadeh, F., Wardle, M., Miller-Jones, J. C. A., et al. 2011, ApJL, 729, 44

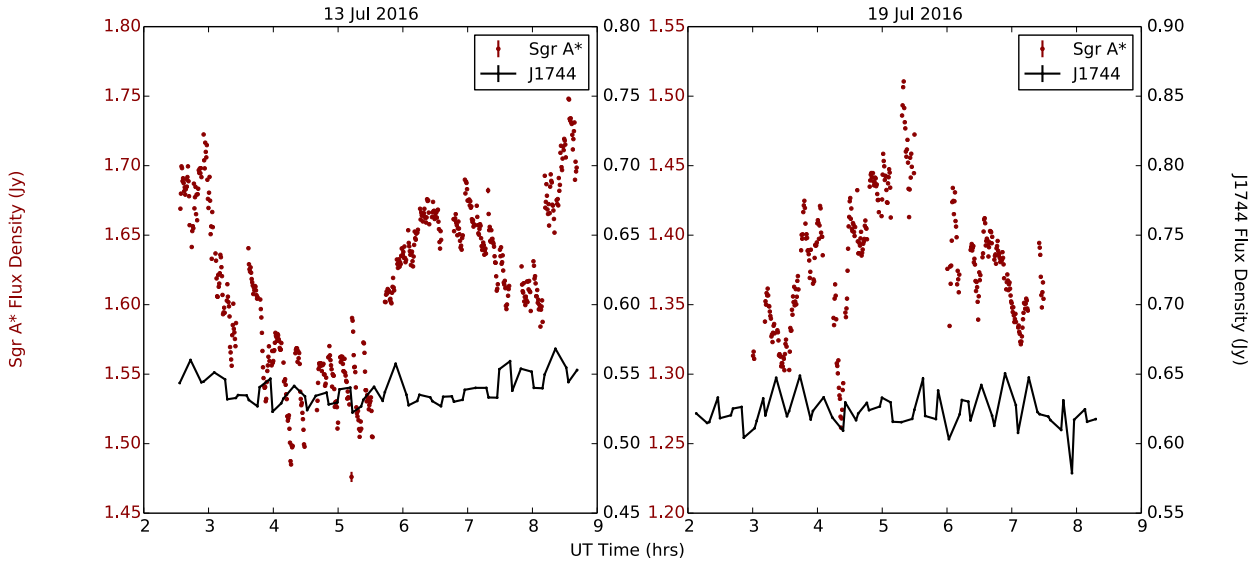

FIG. 2. VLA (long observation) light curves of Sgr A* (red, left axis) and J1744 (black, right axis), taken with 30 and 120 second averaging intervals, respectively. All fluxes were obtained directly from UV data using the AIPS task DFTPL. Note that, due to phase errors, approximately 30 minutes of data were removed on 19 July.

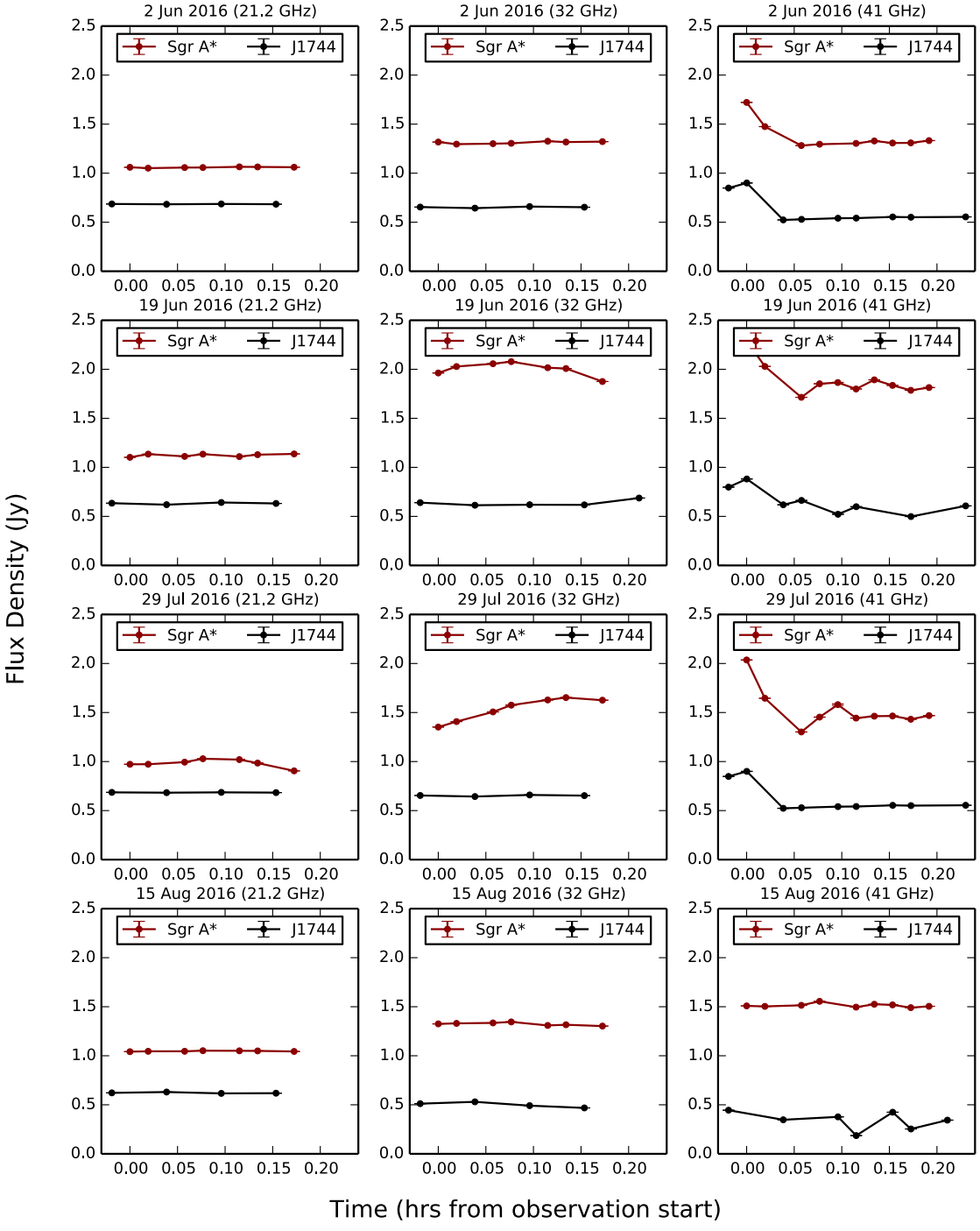

FIG. 3. VLA (short observation) light curves of Sgr A* (red) and J1744 (black), taken with a 60 second averaging interval. Each plot represents a single epoch and frequency band. All fluxes were obtained directly from UV data using the AIPS task DFTPL.

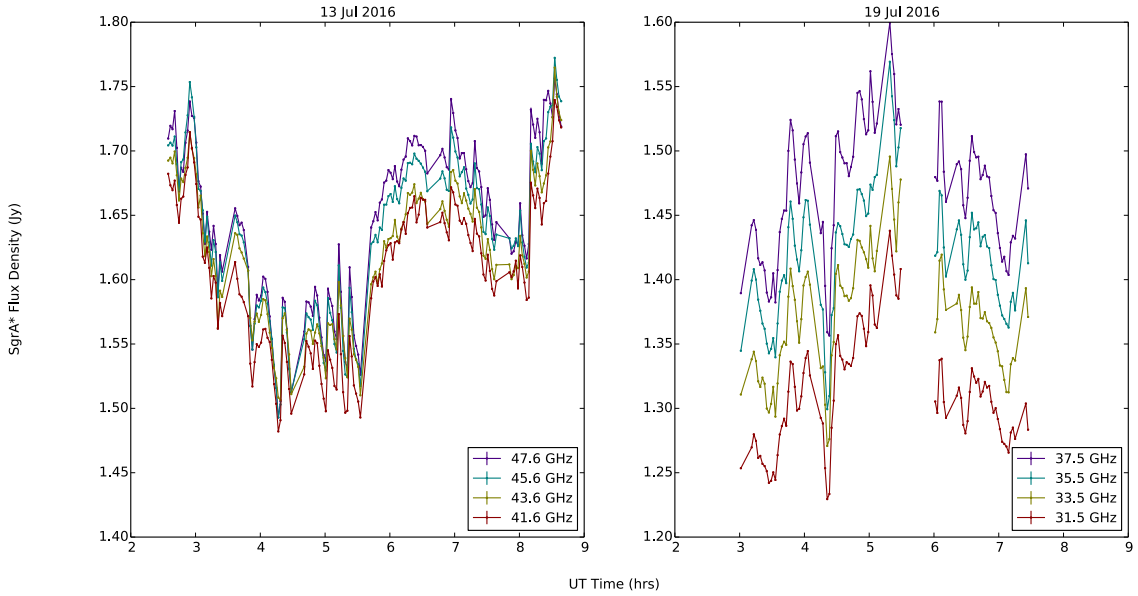

FIG. 4. VLA (long observation) light curves of Sgr A*, taken with a two minute averaging interval. Light curves were taken simultaneously within a given 8 GHz frequency band (Q, or 44 GHz, on 13 July and Ka, o4 34 GHz, on 19 July), and each light curve spans 2 GHz. All fluxes were obtained directly from UV data using the AIPS task DFTPL. Note that, due to phase errors, approximately 30 minutes of data were removed on 19 July.

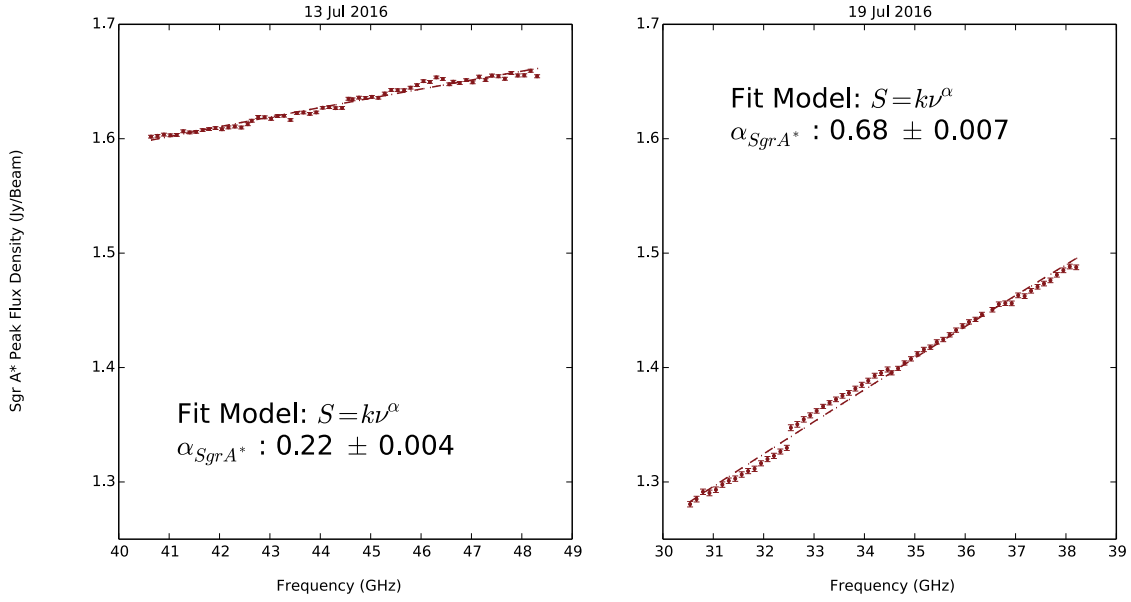

FIG. 5. VLA (long observation) spectra of Sgr A*, with spectral index (α) shown. Spectral indices and fit lines were calculated using least squares regression. All flux densities were obtained by fitting 2D Gaussians in the image plane using the AIPS task JMFIT.

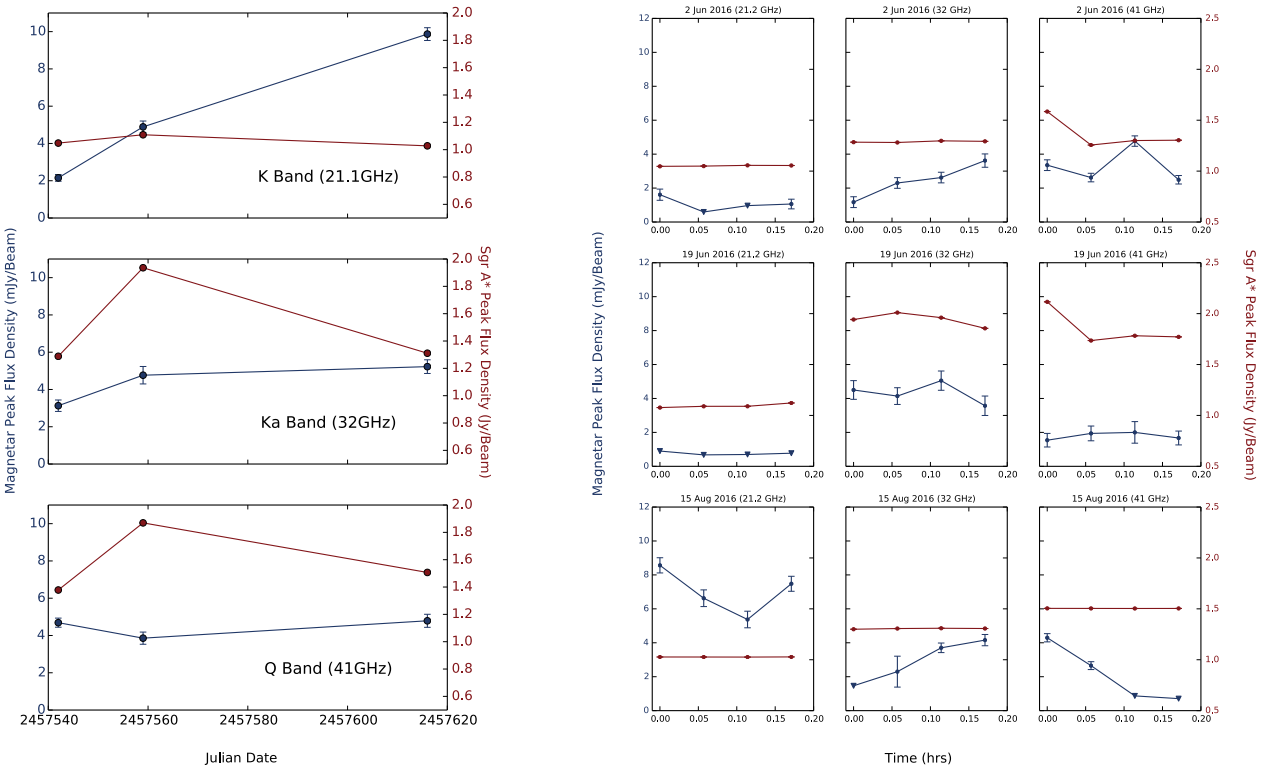

FIG. 6. (a) Left: VLA (snapshot observation) light curves of the magnetar (blue, left axis) and Sgr A* (red, right axis). Three epochs of observations are plotted at three frequencies, 21.2, 32, and 41 GHz. Note that the flux density scale is in mJy beam^{-1} for the magnetar (blue, left hand side) and is in Jy beam^{-1} for Sgr A*. Flux densities were obtained by fitting 2D Gaussians to individual sources in the image plane using the AIPS task JMFIT. (b) Right: Light curves of the magnetar (blue) and Sgr A* (red), taken over the course of each snapshot observation (i.e. each point represents average peak flux density over a two-minute period). Flux densities were again obtained by fitting 2D Gaussians to individual sources in the image plane using the AIPS task JMFIT. Blue triangles indicate one sigma upper limits.

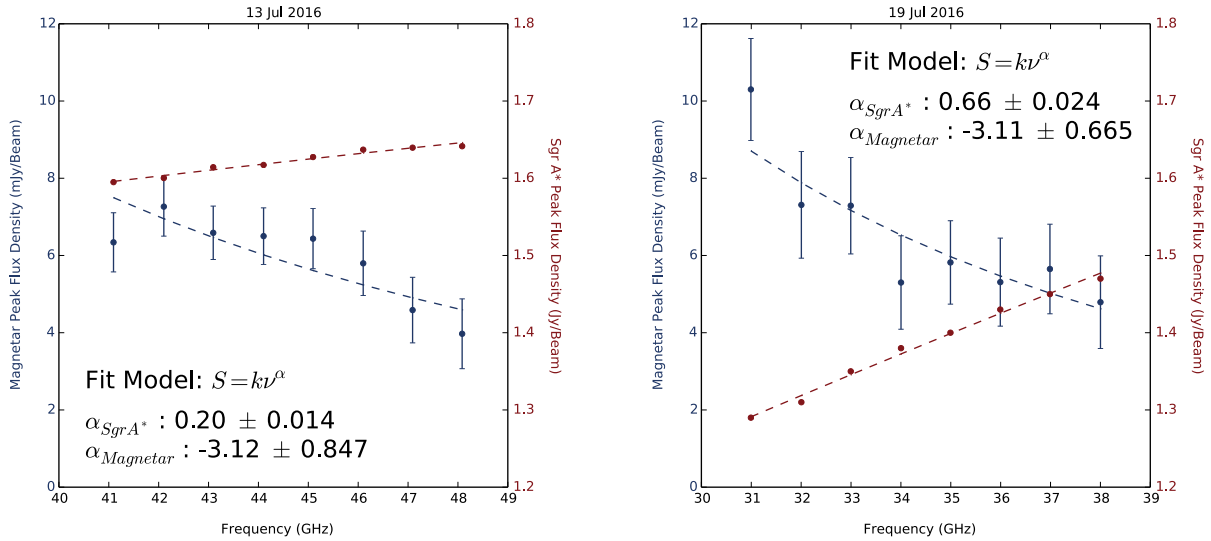

FIG. 7. VLA spectra (long observation) of the magnetar (blue, left axis) and Sgr A* (red, right axis), with spectral indices (α) shown. Spectral indices and fit lines were calculated using least squares regression. Note that, as in Figure 6 the flux density scale is in mJy beam^{-1} for the magnetar (blue, left hand side) and is in Jy beam^{-1} for Sgr A*. Flux densities were obtained by fitting 2D Gaussians to individual sources in the image plane using the AIPS task JMFIT.